

# Multicritical points in the mixed ferromagnetic-ferrimagnetic ternary alloy with a single-ion anisotropy

A. Bobák\* and F. O. Abubrig

*Department of Theoretical Physics and Astrophysics, Faculty of Science, P. J. Šafárik University, Moyzesova 16, 041 54 Košice, Slovak Republic*

T. Balcerzak

*Department of Solid State Physics, University of Łódź, Pomorska 149/153, 90-236 Łódź, Poland*

(Received 14 February 2003; revised manuscript received 17 July 2003; published 4 December 2003)

The phase diagram of the  $AB_pC_{1-p}$  ternary alloy consisting of Ising spins  $S^A = \frac{3}{2}$ ,  $S^B = 1$ , and  $S^C = \frac{5}{2}$  in the presence of a single-ion anisotropy is investigated by the use of a mean-field theory based on the Bogoliubov inequality for the Gibbs free energy. To simulate the structure of the ternary metal Prussian blue analog such as  $(\text{Ni}_p^{\text{II}}\text{Mn}_{1-p}^{\text{II}})_{1.5}[\text{Cr}^{\text{III}}(\text{CN})_6] \cdot z\text{H}_2\text{O}$ , we assume that the A and X (either B or C) ions are alternately connected and the couplings between the A and X ions include both ferromagnetic ( $J_{AB} > 0$ ) and antiferromagnetic ( $J_{AC} < 0$ ) interactions. At the finite temperatures by changing values of the parameters of the model many different types of phase diagrams are obtained, including a variety of multicritical points such as tricritical points, fourth-order point, critical end points, isolated critical points, and triple points.

DOI: 10.1103/PhysRevB.68.224405

PACS number(s): 75.10.Hk, 75.30.Kz, 75.50.Gg

## I. INTRODUCTION

Molecular-based magnets have recently attracted considerable interest in their synthesis and study of the magnetic properties.<sup>1–12</sup> A special class of these materials form the so-called multimetal Prussian blue analogs, such as  $(A_p^{\text{II}}\text{Mn}_{1-p}^{\text{II}})_{1.5}[\text{Cr}^{\text{III}}(\text{CN})_6] \cdot z\text{H}_2\text{O}$  ( $A^{\text{II}} = \text{Ni}^{\text{II}}, \text{Fe}^{\text{II}}$ ) (Refs. 13–15) or  $(\text{Ni}_p^{\text{II}}\text{Mn}_q^{\text{II}}\text{Fe}_r^{\text{II}})_{1.5}[\text{Cr}^{\text{III}}(\text{CN})_6] \cdot z\text{H}_2\text{O}$  (Refs. 16 and 17). These compounds are attractive for the molecular design of magnetic properties because various types of metal ions can be incorporated there as spin centers. Thus, the magnetic properties can be precisely controlled during the synthesis process by changing the ratio of incorporated metal ions (spins).

Up to now, many unusual properties have been discovered in these materials, for instance, the photoinduced magnetization effect,<sup>18,19</sup> magnetic pole inversion,<sup>13,20</sup> inverted magnetic hysteresis loop,<sup>21</sup> and occurrence of one<sup>13,14</sup> or even two<sup>16</sup> compensation points. The theoretical explanation of these phenomena remains an attractive and challenging problem for solid-state physicists.

From the point of view of magnetic classification, the multimetal Prussian blue analogs present ferromagnetic-ferrimagnetic properties, since they include mixed both ferromagnetic ( $J > 0$ ) and antiferromagnetic ( $J < 0$ ) superexchange interactions between the neighboring metal ions through the cyanide bridging ligands. In the description of these materials, a possibility of the application of localized spin models implies that the prediction of magnetic properties is more transparent than in classical metal or metal-oxide magnets, and the theoretical methods are in this case more tractable.

Nevertheless, because of the structural complexity of these systems, the up to now analytical descriptions of their properties have mainly been performed in the simplest approach—namely, in the mean-field approximation

(MFA).<sup>14–17</sup> It is well known that the MFA method allows for complete studies of all thermodynamic properties in a uniform and relatively simply way, based on the Gibbs free energy, and hence is often used for analysis of experimental results.

Another approach, sporadically used for the studies of these systems, the effective field theory,<sup>22</sup> although more accurate than the MFA in the description of continuous phase transitions, does not yield the expression for the Gibbs energy and hence fails in the investigations of complete phase diagrams, where first-order phase transitions can occur. Among other more advanced methods, which could be potentially taken into account, one can mention the cluster variational method in pair approximation.<sup>23</sup> This method, being in a natural way the next step after the MFA in the cumulant expansion scheme for the entropy, has been successfully tested for the complex phase diagrams of the Blume-Emery-Griffiths (BEG) model, giving reliable results based on the free-energy analysis. However, its application for the ternary or quaternary mixed-spin systems with higher spin values, as in the present case, seems to be too complicated.

Thus, at present, among analytical methods, the most practical for the studies of multimetal Prussian blue analogs remains the MFA. Fortunately, the up to now predictions of this method turned out to be in satisfactory agreement with the experiment.<sup>14–16</sup> The additional physical argument for application of the MFA has been formulated in Ref. 17. It says that as far as the exchange interaction between sublattices is greater than the exchange interaction within sublattices, which is the case, the necessary condition for the MFA applicability is satisfied.

Taking this into account, in the present paper we adopt the MFA method for the studies of temperature phase diagrams of the ferromagnetic-ferrimagnetic ternary alloy of the type  $AB_pC_{1-p}$ , consisting of three kinds of magnetic ion: A, B, and C, with different Ising spins  $S^A = \frac{3}{2}$ ,  $S^B = 1$ , and  $S^C = \frac{5}{2}$ , respectively. The structure and the spin values corre-

spond to the Prussian blue analog of the type  $(\text{Ni}_p^{\text{II}}\text{Mn}_{1-p}^{\text{II}})_{1.5}[\text{Cr}^{\text{III}}(\text{CN})_6] \cdot z\text{H}_2\text{O}$  [14]. By the  $p$  parameter, representing the mean proportion of magnetic ions  $B$  and  $C$  which are randomly distributed over the lattice, one can control the type of magnetic ordering and thus the topology of the phase diagrams.

Another important parameter incorporated in the present model is a single-ion anisotropy. It is known that such parameter should be of special interest for spins  $S > 1/2$ , where it can potentially lead to the first-order phase transitions.<sup>23</sup> The influence of the single-ion anisotropy on the ground-state phase diagrams (for  $T=0$  K) has been already investigated in Ref. 24, where the variety of exact results have been obtained. However, as far as the temperature phase diagrams are concerned, such studies have not been done yet for the system in question and, of course, cannot be performed exactly.

It is the aim of the present paper to clarify the influence of the single-ion anisotropy on the temperature phase diagrams of the model ferromagnetic-ferrimagnetic ternary alloy corresponding to the Prussian blue analog, within the MFA method. The studies will be based on the expression for the Gibbs free energy, where the compositional parameter  $p$ , the single-ion anisotropy, the ferromagnetic-ferrimagnetic exchange interaction ratio, as well as the temperature, plays a role. The calculated phase diagrams can be conveniently controlled in the limit  $T \rightarrow 0$  K where, for the ground state, the exact results exist.<sup>24</sup>

The paper is organized as follows. In Sec. II, a precise definition of the model is given and relevant expressions in the mean-field approximation are derived. Section III is devoted to the discussion of the numerical results concerning the temperature phase diagrams. Finally, some conclusions are presented in Sec. IV.

## II. MODEL AND ITS MEAN-FIELD SOLUTION

We consider a ternary alloy of the type  $AB_pC_{1-p}$ , where  $A$  and  $X$  ( $X=B$  or  $C$ ) ions are alternately connected and the couplings between the  $A$  and  $X$  ions include both ferromagnetic ( $J_{AB} > 0$ ) and antiferromagnetic ( $J_{AC} < 0$ ) interactions. Let the  $A$ ,  $B$ , and  $C$  ions have different Ising spins ( $S^A = \frac{3}{2}$ ,  $S^B = 1$ , and  $S^C = \frac{5}{2}$ ), respectively. The Hamiltonian of the system in the presence of a single-ion anisotropy field strength  $D$  and an external magnetic field  $h$  is then of the form

$$H = - \sum_{(i,j)} S_i^A [J_{AB} S_j^B \xi_j + J_{AC} S_j^C (1 - \xi_j)] - D \left[ \sum_{i=1}^{N_A} (S_i^A)^2 + \sum_{j=1}^{N_X} (S_j^B)^2 \xi_j + \sum_{j=1}^{N_X} (S_j^C)^2 (1 - \xi_j) \right] - h \left[ \sum_{i=1}^{N_A} S_i^A + \sum_{j=1}^{N_X} (S_j^B) \xi_j + \sum_{j=1}^{N_X} (S_j^C) (1 - \xi_j) \right], \quad (1)$$

where  $S_i^A = \pm \frac{1}{2}$  and  $\pm \frac{3}{2}$  for  $A$  ions,  $S_j^B = 0$  and  $\pm 1$  for  $B$  ions,  $S_j^C = \pm \frac{1}{2}$ ,  $\pm \frac{3}{2}$ , and  $\pm \frac{5}{2}$  for  $C$  ions, and  $N_A$  and  $N_X$  are the number of sites occupied by the  $A$  and  $X$  ( $X=B$  or  $C$ )

ions, respectively, with  $N_A + N_X = N$  the total number of sites. The first summation is carried out only over nearest-neighbor pairs of spins on different sublattices and  $J_{AB}$  ( $J_{AB} = J_{BA}$ ,  $J_{AB} > 0$ ) and  $J_{AC}$  ( $J_{AC} = J_{CA}$ ,  $J_{AC} < 0$ ) are the nearest-neighbor exchange interactions.  $\xi_j$  is a set of independent, uniformly distributed random variables which take the value of unity or zero, depending on whether the site  $j$  is occupied by an ion of the type  $B$  or  $C$ , respectively. Therefore, the distribution function of  $\xi_j$  is given by

$$P(\xi_j) = p \delta(\xi_j - 1) + q \delta(\xi_j), \quad (2)$$

where  $p$  is the concentration of  $B$  ions and  $q = 1 - p$  is the concentration of  $C$  ions.

We note that the Ising spin model was chosen for this study since Monte Carlo simulations performed on the model for bimetallic molecular-based magnets<sup>25,26</sup> reproduce the results very close to the observed experimentally. Moreover, this model is related to a previously studied one of a simpler nature. Namely, for  $N_A = N_X = N/2$  and  $p = 1$  it reduces to the mixed spin-1 and spin- $\frac{3}{2}$  Ising system,<sup>27,28</sup> while for  $p = 0$  to the mixed spin- $\frac{3}{2}$  and spin- $\frac{5}{2}$  Ising system which has not been studied so far. It is expected that the model may provide an unusually rich laboratory for studying of a number of phase transitions, critical and multicritical phenomena within the framework of one single approach. Therefore, apart from its relevance to the description of a mixed ferromagnetic-ferrimagnetic ternary alloy, this model system is also interesting from a purely theoretical point of view, being among the models able to exhibit multicritical behavior.

The most direct way of deriving the MFA is to use the variation principle for the Gibbs free energy<sup>29</sup>

$$G(H) \leq \phi \equiv G_0(H_0) + \langle \langle H - H_0 \rangle \rangle_c, \quad (3)$$

where  $G(H)$  is the true free energy of the system described by the Hamiltonian (1),  $G_0(H_0)$  is the average free energy of a trial Hamiltonian  $H_0$  which depends on variational parameters,  $\langle \dots \rangle_0$  denotes a thermal average over the ensemble defined by  $H_0$ , and  $\langle \dots \rangle_c$  indicates the configurational average using the distribution function given by Eq. (2).

To obtain the MFA, we assume the trial Hamiltonian in the form

$$H_0 = - \sum_{i=1}^{N_A} [(\gamma_A + h) S_i^A + D (S_i^A)^2] - \sum_{j=1}^{N_X} \{ (\gamma_B + h) \xi_j S_j^B + (\gamma_C + h) (1 - \xi_j) S_j^C + D [\xi_j (S_j^B)^2 + (1 - \xi_j) (S_j^C)^2] \}, \quad (4)$$

where  $\gamma_A$ ,  $\gamma_B$ , and  $\gamma_C$  are the three variational parameters related to molecular fields acting on the three different spins, respectively.

Because of the simplicity of  $H_0$  it is easy to evaluate the expressions in Eq. (3) and we finally obtain

$$\begin{aligned}
g \equiv \frac{\phi}{N} = & -\frac{N_A}{N} k_B T \ln \left\{ 2 \exp\left(\frac{1}{4}\beta D\right) \cosh\left[\frac{1}{2}\beta(\gamma_A+h)\right] + 2 \exp\left(\frac{9}{4}\beta D\right) \cosh\left[\frac{3}{2}\beta(\gamma_A+h)\right] \right\} \\
& -\frac{N_X}{N} p k_B T \ln \{ 2 \exp(\beta D) \cosh[\beta(\gamma_B+h)] + 1 \} - \frac{N_X}{N} (1-p) k_B T \ln \left\{ 2 \exp\left(\frac{1}{4}\beta D\right) \cosh\left[\frac{1}{2}\beta(\gamma_C+h)\right] \right. \\
& \left. + 2 \exp\left(\frac{9}{4}\beta D\right) \cosh\left[\frac{3}{2}\beta(\gamma_C+h)\right] + 2 \exp\left(\frac{25}{4}\beta D\right) \cosh\left[\frac{5}{2}\beta(\gamma_C+h)\right] \right\} - \frac{N_A}{N} z_1 (J_{AB} m_B + J_{AC} m_C) m_A + \frac{N_A}{N} \gamma_A m_A \\
& + \frac{N_X}{N} (\gamma_B m_B + \gamma_C m_C), \tag{5}
\end{aligned}$$

where  $\beta = 1/k_B T$  and the sublattice magnetizations per site  $m_A, m_B$ , and  $m_C$  are defined by

$$m_A \equiv \langle \langle S_i^A \rangle_0 \rangle_c = \frac{1}{2} \frac{3 \sinh\left[\frac{3}{2}\beta(\gamma_A+h)\right] + \delta^2 \sinh\left[\frac{1}{2}\beta(\gamma_A+h)\right]}{\cosh\left[\frac{3}{2}\beta(\gamma_A+h)\right] + \delta^2 \cosh\left[\frac{1}{2}\beta(\gamma_A+h)\right]}, \tag{6}$$

$$m_B \equiv \langle \langle S_j^B \rangle_0 \xi_j \rangle_c = p \frac{2 \sinh[\beta(\gamma_B+h)]}{2 \cosh[\beta(\gamma_B+h)] + \delta}, \tag{7}$$

$$m_C \equiv \langle \langle S_j^C \rangle_0 (1 - \xi_j) \rangle_c = \frac{(1-p)}{2} \frac{5 \sinh\left[\frac{5}{2}\beta(\gamma_C+h)\right] + 3 \delta^4 \sinh\left[\frac{3}{2}\beta(\gamma_C+h)\right] + \delta^6 \sinh\left[\frac{1}{2}\beta(\gamma_C+h)\right]}{\cosh\left[\frac{5}{2}\beta(\gamma_C+h)\right] + \delta^4 \cosh\left[\frac{3}{2}\beta(\gamma_C+h)\right] + \delta^6 \cosh\left[\frac{1}{2}\beta(\gamma_C+h)\right]}, \tag{8}$$

where  $\delta = \exp(-\beta D)$ . It should be noted here that in deriving of Eq. (5), we have used the relation

$$z_1 N_A = z_2 N_X, \tag{9}$$

where  $z_1$  and  $z_2$  are the numbers of the nearest neighbors of the A and X ( $X=B$  or  $C$ ) ions, respectively. The values of  $z_1$  and  $z_2$  are fixed and controlled by the stoichiometry of the system. In the case of the above-mentioned Prussian-blue-like compound, which for X/A displays a 3:2 stoichiometry, there is  $z_1=6$  and  $z_2=4$  (Ref. 14).

Now, by minimizing the free energy (5) with respect to  $\gamma_A, \gamma_B$ , and  $\gamma_C$ , we determine these parameters in the form

$$\begin{aligned}
\gamma_A &= z_1 (J_{AB} m_B + J_{AC} m_C), & \gamma_B &= z_2 J_{AB} m_A, \\
\gamma_C &= z_2 J_{AC} m_A. \tag{10}
\end{aligned}$$

The mean-field properties of the present system are then given by Eqs. (5)–(8) and (10). For example, the total magnetization per site is obtained from the free energy:

$$M = -\frac{\partial g_{\min}}{\partial h} = \frac{1}{N} [N_A m_A + N_X (m_B + m_C)]. \tag{11}$$

There can be, in general, several triplets of solution ( $m_A, m_B, m_C$ ) for Eqs. (6)–(8), and the triplet chosen is that which minimizes the free energy in Eq. (5). So the detailed analysis of the phase diagrams must be performed numerically. Nevertheless, some parts of the phase diagrams can be discussed analytically. For instance, close to the second-

order phase transition from the ordered state ( $m_A \neq 0, m_B \neq 0, m_C \neq 0$ ) to the paramagnetic one ( $m_A = m_B = m_C = 0$ ), the sublattice magnetizations  $m_A, m_B$ , and  $m_C$  are very small, for  $h=0$ , and we may expand Eqs. (6)–(8) into the form

$$m_A = A_1 \gamma_A + A_2 \gamma_A^3 + A_3 \gamma_A^5 + A_4 \gamma_A^7 + \dots, \tag{12}$$

$$m_B = B_1 \gamma_B + B_2 \gamma_B^3 + B_3 \gamma_B^5 + B_4 \gamma_B^7 + \dots, \tag{13}$$

$$m_C = C_1 \gamma_C + C_2 \gamma_C^3 + C_3 \gamma_C^5 + C_4 \gamma_C^7 + \dots, \tag{14}$$

where the coefficients  $A_i, B_i$ , and  $C_i$  ( $i=1-4$ ) are functions of  $\beta, D$ , and  $p$ . These coefficients, because of their complexity, are not given here. Now, by substituting Eqs. (13) and (14) into Eq. (12) and retaining the terms until  $m_A^7$ , one obtains

$$m_A = a m_A + b m_A^3 + c m_A^5 + d m_A^7 + \dots, \tag{15}$$

where, for instance, the coefficient  $a$  is given by

$$\begin{aligned}
a = & \frac{1}{4} z_1 z_2 (\beta J_{AB})^2 \frac{9 + \delta^2}{1 + \delta^2} \left[ \frac{2p}{2 + \delta} \right. \\
& \left. + \frac{(1-p)}{4} \frac{25 + 9\delta^4 + \delta^6}{1 + \delta^4 + \delta^6} R^2 \right], \tag{16}
\end{aligned}$$

with  $R = |J_{AC}|/J_{AB}$ .

In this way, critical and some multicritical points are determined as follows<sup>27</sup>: (i) second-order transition lines occur when  $a=1$  and  $b<0$ , (ii) tricritical points when  $a=1$ ,  $b=0$ , and  $c<0$ , and (iii) fourth-order points when  $a=1$ ,  $b=0$ ,  $c=0$ , and  $d<0$ . Note that we have found that the seventh-order coefficient  $d$  in the expansion (15) is negative in the entire  $(T,D,p,R)$  space and thus the highest-order multicritical entity in this system is the fourth-order point.

### III. RESULTS AND DISCUSSION

In this section we shall present and discuss the results we have obtained for the temperature phase diagrams, together with the temperature dependence of the sublattice magnetizations (just in some most interesting cases). However, for the sake of completeness, we begin with a brief discussion of the ground state which is relevant for understanding of the phase diagrams at finite temperature.

At zero temperature, because of the competing effect between exchange interactions and negative single-ion anisotropy strength, possible ground states in a  $[S^A, S^B, S^C]$  representation are  $[\frac{3}{2}, 1, -\frac{5}{2}]$ ,  $[\frac{3}{2}, 1, -\frac{3}{2}]$ ,  $[\frac{3}{2}, 1, -\frac{1}{2}]$ ,  $[\frac{3}{2}, 0, -\frac{5}{2}]$ ,  $[\frac{3}{2}, 0, -\frac{3}{2}]$ ,  $[\frac{1}{2}, 1, -\frac{1}{2}]$ ,  $[\frac{1}{2}, 0, -\frac{5}{2}]$ ,  $[\frac{1}{2}, 0, -\frac{3}{2}]$ , and  $[\frac{1}{2}, 0, -\frac{1}{2}]$ , for  $p \neq 0$  and  $p \neq 1$ . On the other hand, for  $p=0$  and  $p=1$  the ground states are  $[S^A, S^C] \equiv [\frac{3}{2}, -\frac{5}{2}]$  or  $[\frac{3}{2}, -\frac{3}{2}]$  or  $[\frac{1}{2}, -\frac{1}{2}]$  and  $[S^A, S^B] \equiv [\frac{3}{2}, 1]$  or  $[\pm\frac{1}{2}, 0]$ , respectively. The latter state, which appears below  $D/J_{AB} = -18/7 \approx -2.5714$ , for any  $R$ , corresponds to the disordered phase: The spins  $S^B$  are in the  $S^B=0$  state, while the spins on sublattice A are in states  $S^A = \pm\frac{1}{2}$ , distributed at random, with equal probabilities. Which one of the above states is the actual ground state depends on the values of the three parameters  $R = |J_{AC}|/J_{AB}$ ,  $D$ , and  $p$  in the ground-state energy obtained from the Hamiltonian (1). Different values of  $p$  therefore lead to different ground-state phase diagrams in the  $R$ - $D$  plane. The boundaries between the regions in this plane that correspond to a particular ground state are obtained by pairwise equating the ground-state energies of neighboring phases. A detailed discussion of the topology of the ground-state phase diagrams has been already presented in Ref. 24.

Let us now turn to the finite-temperature phase diagrams of the system in the  $D$ - $T$  plane obtained for different values of the concentration  $p$  and the interaction ratio  $R$ . While second-order phase transition lines are easily obtained from Eq. (16) by setting  $a=1$ , first-order phase transition lines must be determined by comparing the corresponding free energies of the various solutions of Eqs. (6)–(8) for the triplet  $(m_A, m_B, m_C)$ .

In particular, at  $D=0$ , the critical temperature  $T_c$  is given by

$$\frac{k_B T_c}{J_{AB}} = \frac{1}{4} \left\{ \frac{5}{3} z_1 z_2 [8p + 35(1-p)R^2] \right\}^{1/2}. \quad (17)$$

In Fig. 1, we show the variations of  $T_c$  as a function of  $R$  for different concentrations  $p$  ( $q=1-p$ ) of  $B$  ( $C$ ) atoms. The straight lines with  $p=1$  and  $p=0.0$  correspond to the critical temperatures of the mixed-spin systems with  $S^A = \frac{3}{2}$ ,  $S^B = 1$

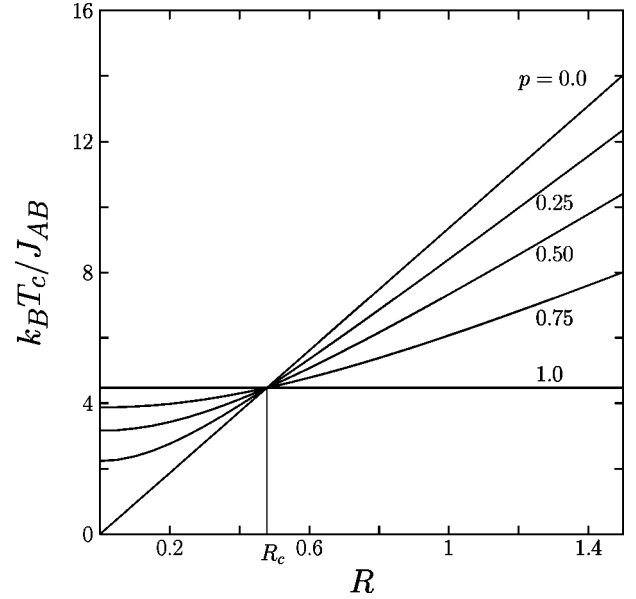


FIG. 1. Phase diagram in the  $R$ - $T$  plane for the ternary alloy  $AB_pC_{1-p}$ , when the concentration  $p$  is changed.

and  $S_A = \frac{3}{2}$ ,  $S^C = \frac{5}{2}$ , respectively. For the former system with  $z_1 = z_2 \equiv z$  one recovers  $k_B T_c / z J_{AB} = (5/6)^{1/2} \approx 0.9129$ , as in Ref. 28, while for the latter system we obtain  $k_B T_c / z |J_{AC}| = (5/4)(7/3)^{1/2} \approx 1.9094$  which is nothing else than the critical temperature of the mixed spin- $\frac{3}{2}$  and spin- $\frac{5}{2}$  Ising system on a lattice with coordination number  $z$ , in our approximation. Thus, by varying  $p$ , we can realize a magnetic crossover from the ferromagnetic mixed spin- $\frac{3}{2}$  and spin-1 to the ferromagnetic mixed spin- $\frac{3}{2}$  and spin- $\frac{5}{2}$  system. Further, it is easy to see from this figure that for  $p > 1.0$  there exists a critical value of the exchange interaction ratio  $R_c = (8/35)^{1/2} \approx 0.4781$  such that, when  $R > R_c$ , the critical temperature of the ternary alloy is higher than that of the mixed spin- $\frac{3}{2}$  and spin-1 Ising system. As seen from Eq. (17), the value of  $R_c$ , at least within the mean-field theory, does not depend on the nearest-neighbor coordination number. On the other hand, if we fix  $R=0$ , we have a mixed spin- $\frac{3}{2}$  and spin-1 Ising system with dilution of the  $B$  sublattice (i.e., the sublattice consisting of the spin-1 ions). In this case, we can observe that the transition temperature gradually reduces from  $k_B T_c / J_{AB} = (1/2)(10z_1 z_2 / 3)^{1/2} \approx 4.4721$  at  $p=1$  (or  $q \equiv 1-p=0$ ) to  $k_B T_c / J_{AB} = 0$  at the mean-field critical concentration  $p_c = 0$ .

In Fig. 2, we present the critical temperature of the ternary alloy as a function of  $p$  for various values of  $R$ . The horizontal line corresponds to the case of  $R \equiv R_c = 0.4781$ , such that  $k_B T_c / J_{AB} = 4.4721$ . In other words, the critical temperature of the mixed spin- $3/2$  and spin-1 Ising system for  $R = 0.4781$  is equal to that of the mixed spin- $\frac{3}{2}$  and spin- $\frac{5}{2}$  Ising one. Thus, in this special case the critical temperature of the system is not changed even when the spin-1 ions are substituted by the spin- $\frac{5}{2}$  ions. It is also noteworthy that the value of  $R_c = 0.4781$  is very close to the  $R$  value of 0.45 considered in the experimental study of the ternary metal Prussian blue analog  $(\text{Ni}_p^{\text{II}}\text{Mn}_{1-p}^{\text{II}})_{1.5}[\text{Cr}^{\text{III}}(\text{CN})_6] \cdot z\text{H}_2\text{O}$ .<sup>14</sup> Further, it is seen from Fig. 2 that, for  $0 < R < R_c$ , the critical

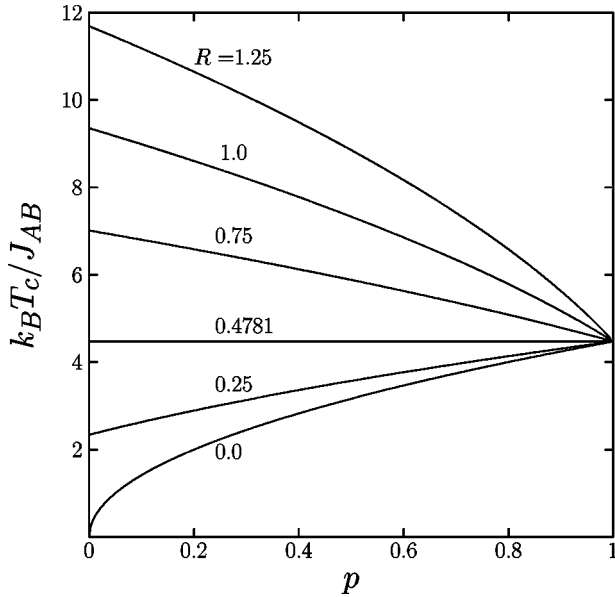


FIG. 2. Phase diagram in the  $p$ - $T$  plane for the ternary alloy  $AB_p C_{1-p}$ , when the interaction ratio  $R$  is changed.

temperature of the ternary alloy is smaller than that of the mixed spin- $\frac{3}{2}$  and spin-1 system and decreases with the decrease of  $p$  to reach its minimum value at  $p=0$ . Moreover, if  $R=0.0$ , then we have a mixed-spin system with  $S^A = \frac{3}{2}$ ,  $S^B = 1$  when only one ( $B$ ) sublattice is being diluted. In this case, the critical temperature vanishes at the mean-field critical concentration  $p_c=0$ , as noted above. On the other hand, for  $R > R_c$ , the critical temperature of the ternary alloy is higher than that of the mixed spin- $\frac{3}{2}$  and spin-1 system and increases with the decrease of  $p$  to reach its maximum value at  $p=0$ .

Let us now turn our attention to the phase diagrams obtained in the  $D$ - $T$  plane for different values of  $p$ , while we restrict ourselves to the  $R \equiv R_c = 0.4781$  (as mentioned above, this value of  $R$  is very close to that considered in the experimental work<sup>14</sup>).

For  $p=1$ , a phase diagram topology with a tricritical point ( $T$ ), a triple point ( $Tr$ ), and isolated critical point ( $C$ ) appears as shown in Fig. 3. The  $[\frac{3}{2}, 1]$  ordered and paramagnetic ( $P$ ) phases are separated at low temperatures by a first-order transition line starting at  $D/J_{AB} = -2.5714$  in agreement with the ground state discussed briefly above. On the higher-temperature segment of this first-order line (above the triple point) the  $[\frac{3}{2}, 1]$  and  $[\pm \frac{1}{2}, 0]$  phases coexist, and at the isolated critical point the two phases coalesce.

Typical sublattice magnetization curves  $m_A$  and  $m_B$ , which correspond to the value of  $D/J_{AB} = -2.4$ , where the  $[\frac{3}{2}, 1] \leftrightarrow [\pm \frac{1}{2}, 0]$  first-order transition occurs at  $T > 0$  K, are plotted in Fig. 4, where the first-order transition is indicated by a vertical dashed line. It should be noted here that the nonzero solution for the sublattice magnetizations in the  $[\pm \frac{1}{2}, 0]$  phase becomes unstable at low temperatures (below the first-order transition) and vanishes at  $T=0$  K in agreement with the ground-state phase diagram.<sup>24</sup> Therefore, this higher-temperature ordered phase comes into existence from

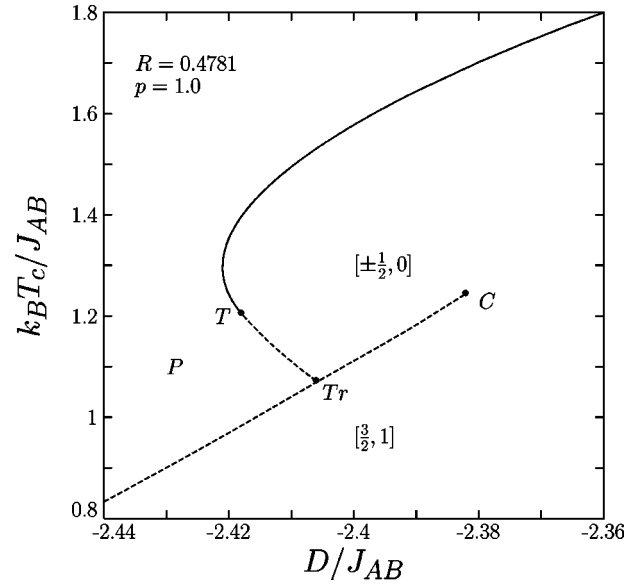


FIG. 3. Phase diagram of the ternary alloy  $AB_p C_{1-p}$  for  $R = 0.4781$  and  $p = 1.0$  with a tricritical point  $T$ , a triple point  $Tr$ , and an isolated critical point  $C$ . The solid and dashed lines indicate second- and first-order phase transitions, respectively.  $[\frac{3}{2}, 1]$  and  $[\pm \frac{1}{2}, 0]$  are ordered ferromagnetic phases and  $P$  is the paramagnetic phase.

the ground-state  $[\pm \frac{1}{2}, 0]$  disordered phase. In other words, the  $[\pm \frac{1}{2}, 0]$  ground state turns, as  $D/J_{AB}$  increases, into an ordered ferrimagnetic phase, which has been denoted in Fig. 3 again by the same symbol—i.e.,  $[\pm \frac{1}{2}, 0]$ . We envision the following origin of  $m_A \neq 0$  and  $m_B \neq 0$  in the  $[\pm \frac{1}{2}, 0]$  ordered phase: For  $D/J_{AB} > -2.4217$ , the  $S^B = +1$  (or  $-1$  as well) spin states on sublattice  $B$  may be populated at  $T \neq 0$  K,

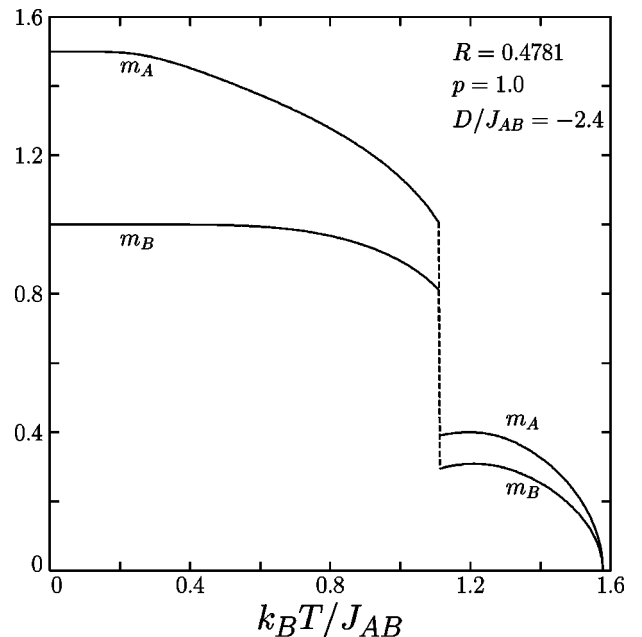


FIG. 4. The thermal dependences of the sublattice magnetizations  $m_A$  and  $m_B$  for the ternary alloy  $AB_p C_{1-p}$  with  $R = 0.4781$ ,  $p = 1.0$ , and  $D/J_{AB} = -2.4$ .

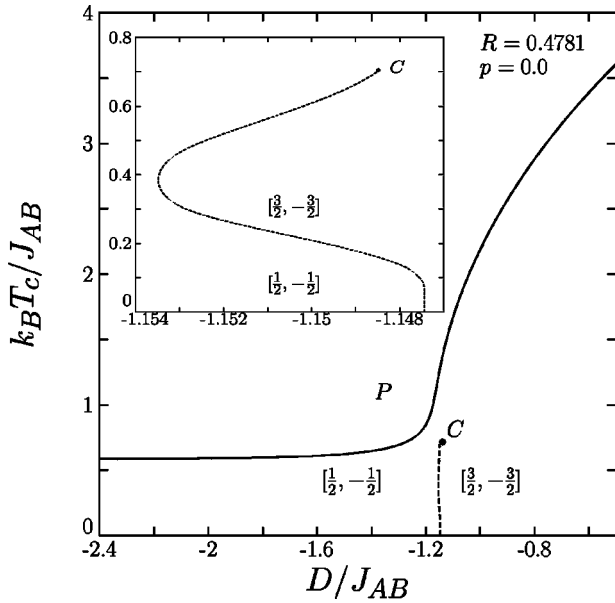


FIG. 5. Phase diagram of the ternary alloy  $AB_p C_{1-p}$  for  $R = 0.4781$  and  $p = 0.0$  with an isolated critical point  $C$ . The solid and dashed lines indicate second- and first-order phase transitions, respectively.  $[\frac{1}{2}, -\frac{1}{2}]$  and  $[\frac{3}{2}, -\frac{3}{2}]$  are ordered ferrimagnetic phases and  $P$  is the paramagnetic phase. The inset shows the first-order transitions in the low-temperature region on an enlarged scale.

which simply corresponds to the introduction of magnetic atoms in the sublattice  $B$ , since they are active as regards producing ferromagnetic ordering. This group of spins is then connected by the nearest-neighbor bonds with spins belonging to the sublattice  $A$ , forming an infinite cluster which can be ordered at higher temperature. Of course, this is the mean-field behavior and, therefore, it would be also interesting to check whether this phase indeed emerges in the system by using alternative technique (Monte Carlo, renormalization group).

Further, it is seen from Fig. 3 that at  $-2.4217 < D/J_{AB} < -2.4060$  there is a reentrant behavior; i.e., the  $P - [\pm \frac{1}{2}, 0] - P$  sequence of phases is encountered as temperature is lowered. The phenomenon may be caused by the competition between the exchange interaction and negative single-ion anisotropy strength.

On the other hand, for  $p = 0$  and  $R = 0.4781$ , no tricritical and triple points are found (Fig. 5) and the second-order transition line between ferrimagnetic and paramagnetic phases extends to  $D/J_{AB} \rightarrow -\infty$ . Moreover, there is a line of first-order transitions situated within ferrimagnetically ordered region, separating the  $[\frac{1}{2}, -\frac{1}{2}]$  and  $[\frac{3}{2}, -\frac{3}{2}]$  phases and terminating at an isolated critical point ( $C$ ) at which the ordered phases coalesce. We note that the line of first-order transitions exhibits a small reentrant behavior (see inset of Fig. 5) and goes to zero temperature at a value of  $D/J_{AB}$  corresponding to  $D/J_{AB} = -(12/5)R$ , which is on the boundary of the  $[\frac{3}{2}, -\frac{3}{2}]$  and  $[\frac{1}{2}, -\frac{1}{2}]$  phases in the ground state. The lines of transitions from Fig. 5 are reminiscent of those occurring in the spin- $\frac{3}{2}$  Blume-Capel model.<sup>30,31</sup> It is also noteworthy that, for  $p = 0$  and  $R = 0.4781$ , there is no finite-

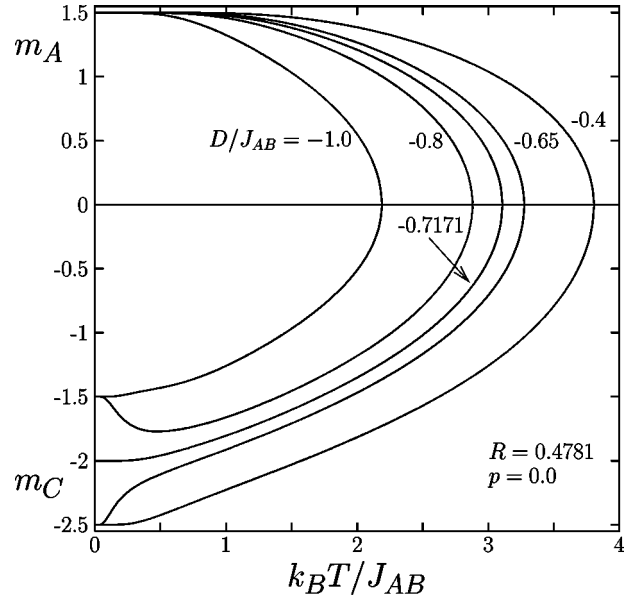


FIG. 6. The thermal dependences of the sublattice magnetizations  $m_A$  and  $m_C$  for the ternary alloy  $AB_p C_{1-p}$  with  $R = 0.4781$  and  $p = 0.0$ , when the value of  $D/J_{AB}$  is changed.

temperature transition between the  $[\frac{3}{2}, -\frac{3}{2}]$  and  $[\frac{3}{2}, -\frac{5}{2}]$  phases, but only at zero temperature in the first-order transition point between them, at  $D/J_{AB} \approx -0.7171$ , the new phase emerges characterized by the  $[\frac{3}{2}, -2]$  state. (Due to the lack of space the symbols,  $[\frac{3}{2}, -\frac{5}{2}]$  and  $[\frac{3}{2}, -2]$  are omitted in Fig. 5.) It indicates that at this point in the ground state the spin configuration of  $S_j^C$  in the system consists of the mixed state; half of the spins on the sublattice  $C$  are equal to  $-\frac{5}{2}$  (or  $+\frac{5}{2}$  as well) and the other half are equal to  $-\frac{3}{2}$  (or  $+\frac{3}{2}$  as well). It is seen from Fig. 6 that the  $C$  sublattice magnetization curves for values of  $D/J_{AB}$  from both sides of the point where the mixed state occurs may exhibit some unusual features. For values of  $D/J_{AB}$  slightly below  $-0.7171$ , the magnetization curve  $|m_C|$  may exhibit a rather rapid increase from its saturation value at  $T = 0$  K, while for values of  $D/J_{AB}$  slightly above  $-0.7171$  there is a rapid decrease of  $|m_C|$  from the saturation value with the increase in  $T$ . On the other hand, for all values of  $D/J_{AB}$  the sublattice magnetization  $m_A$  may show normal behavior, even though it is coupled to  $m_C$ .

We now turn to the situation when  $0 < p < 1$  and  $R = 0.4781$ . In this case we obtain five topologically different types of phase diagrams reported in Figs. 7–10.

In Fig. 7, for  $p = 0.8$ , the two ordered phases are separated, at low temperatures, by a first-order transition line, starting at  $D/J_{AB} \approx -2.3396$ , at  $T = 0$  K, corresponding to  $D/J_{AB} = -6[3p + R(1-p)]/(4+3p)$ , which is on the boundary of the  $[\frac{3}{2}, 1, -\frac{1}{2}]$  and  $[\frac{1}{2}, 0, -\frac{1}{2}]$  phases in the ground state. The  $[\frac{1}{2}, 0, -\frac{1}{2}]$  ordered phase terminates at a second-order transition line which starts from a critical end point ( $E$ ) and extends to  $D/J_{AB} \rightarrow -\infty$ . The higher-temperature segment of the first-order line above a triple point ( $Tr$ ), on which two ordered phases again coexist, ter-

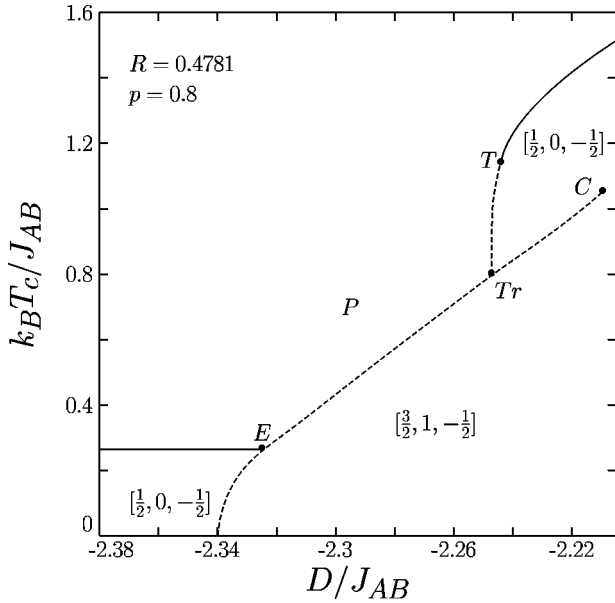


FIG. 7. Phase diagram of the ternary alloy  $AB_pC_{1-p}$  for  $R = 0.4781$  and  $p=0.8$  with a tricritical point  $T$ , a triple point  $Tr$ , a critical end point  $E$ , and an isolated critical point  $C$ . The solid and dashed lines indicate second- and first-order phase transitions, respectively.  $[\frac{1}{2}, 0, -\frac{1}{2}]$  and  $[\frac{3}{2}, 1, -\frac{1}{2}]$  are ordered ferrimagnetic phases and  $P$  is the paramagnetic phase.

minates itself at a isolated critical point ( $C$ ). This higher-temperature picture is similar to that for  $p=1.0$ , with except that now a reentrant behavior does not occur. It should be noted here that for increasing  $D/J_{AB}$  from  $D/J_{AB} \approx -2.3396$ , when the sequence of ground states for  $R$

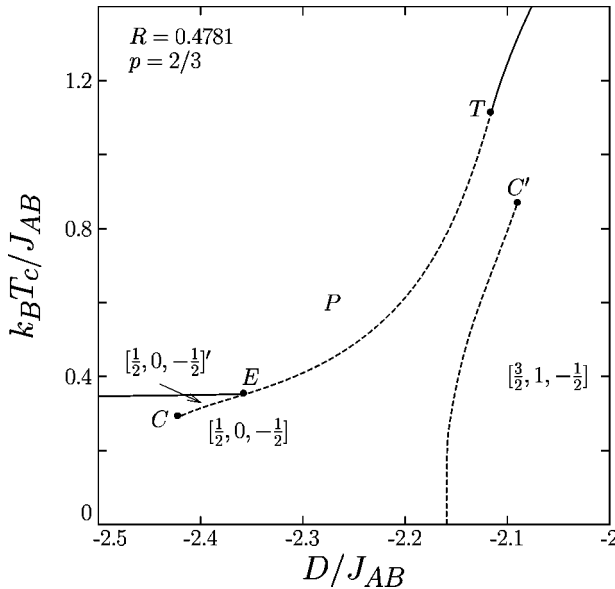


FIG. 8. Phase diagram of the ternary alloy  $AB_pC_{1-p}$  for  $R = 0.4781$  and  $p=2/3$  with a tricritical point  $T$ , a critical end point  $E$ , and two isolated critical points  $C, C'$ . The solid and dashed lines indicate second- and first-order phase transitions, respectively.  $[\frac{1}{2}, 0, -\frac{1}{2}]$ ,  $[\frac{1}{2}, 0, -\frac{1}{2}]'$ , and  $[\frac{3}{2}, 1, -\frac{1}{2}]$  are ordered ferrimagnetic phases and  $P$  is the paramagnetic phase.

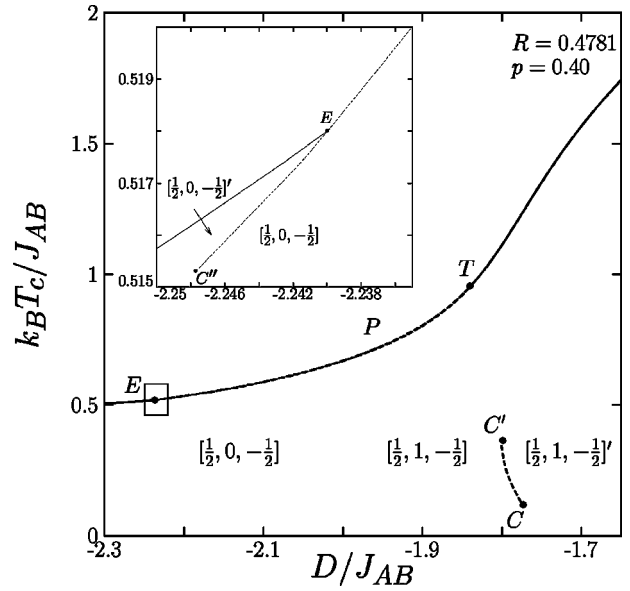


FIG. 9. Phase diagram of the ternary alloy  $AB_pC_{1-p}$  for  $R = 0.4781$  and  $p=0.4$  with a tricritical point  $T$ , a critical end point  $E$ , and three isolated critical points  $C, C', C''$ . The solid and dashed lines indicate second- and first-order phase transitions, respectively.  $[\frac{1}{2}, 0, -\frac{1}{2}]$ ,  $[\frac{1}{2}, 0, -\frac{1}{2}]'$ ,  $[\frac{1}{2}, 1, -\frac{1}{2}]$ , and  $[\frac{1}{2}, 1, -\frac{1}{2}]'$  are ordered ferrimagnetic phases and  $P$  is the paramagnetic phase. The inset shows a closer view in the boxed region around the critical end point  $E$ .

$= 0.4781$  is  $[\frac{3}{2}, 1, -\frac{1}{2}]$ ,  $[\frac{3}{2}, 1, -\frac{3}{2}]$ , and  $[\frac{3}{2}, 1, -\frac{5}{2}]$  (see Ref. 24), there occur on the boundaries between different phases only mixed-spin states, likewise in the case of  $p=0.0$ . Such mixed-spin states in the ground state are also observed on the

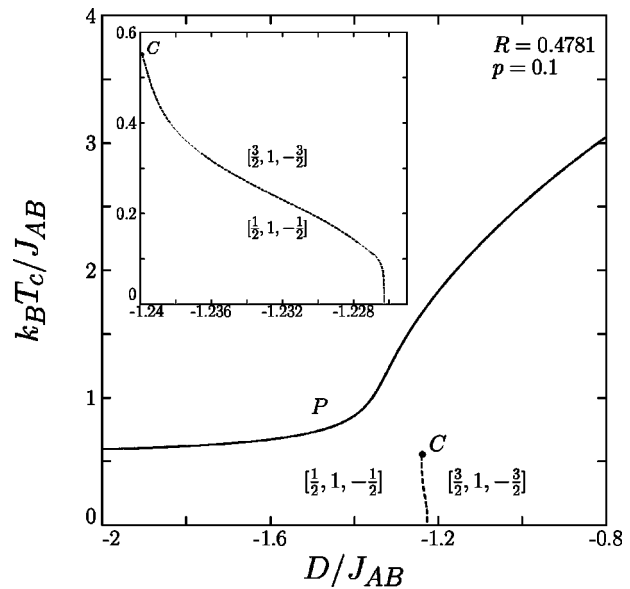


FIG. 10. Phase diagram of the ternary alloy  $AB_pC_{1-p}$  for  $R = 0.4781$  and  $p=0.1$  with an isolated critical point  $C$ . The solid and dashed lines indicate second- and first-order phase transitions, respectively.  $[\frac{1}{2}, 1, -\frac{1}{2}]$  and  $[\frac{3}{2}, 1, -\frac{3}{2}]$  are ordered ferrimagnetic phases and  $P$  is the paramagnetic phase. The inset shows the first-order transitions in the low-temperature region on an enlarged scale.

boundaries between different phases for another values of  $p$  considered below; however, we will not discuss them.

For  $p=2/3$ , a new type of phase diagram appears (Fig. 8) in which the first-order transition line separating the ordered and paramagnetic phases and starting at a tricritical point ( $T$ ), meets the second-order transition line at a critical end point ( $E$ ) and terminates at an isolated critical point ( $C$ ) inside the ordered phase. Thus in this case, the  $[\frac{1}{2}, 0, -\frac{1}{2}]$  ordered phase exhibits distinct dense and dilute versions coexisting on the low-temperature segment of the first-order line. In addition, there is another line of first-order transitions that separates the  $[\frac{1}{2}, 0, -\frac{1}{2}]$  and  $[\frac{3}{2}, 1, -\frac{1}{2}]$  phases and terminates at an isolated critical point ( $C'$ ). This line starts at zero temperature at value of  $D/J_{AB} \approx -2.1594$  again given by  $D/J_{AB} = -6[3p + R(1-p)]/(4+3p)$ .

As  $p$  is lowered, we obtain a phase diagram (Fig. 9) with two first-order line segments inside the ferrimagnetic phase, on which two ferrimagnetic phases—namely, the  $[\frac{1}{2}, 1, -\frac{1}{2}]$  and  $[\frac{1}{2}, 0, -\frac{1}{2}]$  phases—exhibit distinct densities (different sublattice magnetizations at nonzero temperature). It is seen from Fig. 9 that the first-order  $[\frac{1}{2}, 1, -\frac{1}{2}]/[\frac{1}{2}, 1, -\frac{1}{2}]'$  boundary rises from an isolated critical point ( $C$ ) at a low temperature and terminates at another isolated critical point ( $C'$ ). On the other hand, the first-order line segment, on which the  $[\frac{1}{2}, 0, -\frac{1}{2}]$  and  $[\frac{1}{2}, 0, -\frac{1}{2}]'$  phases coexist, starts at an isolated critical point ( $C''$ ) and meets the second-order transition line at the critical end point ( $E$ ) (see the inset of Fig. 9). These coexisting phases, four in number when sublattice magnetizations  $\pm(m_A, m_B, m_C)$  and  $\pm(m'_A, m'_B, m'_C)$  are taken into account, are the phases that become mutually critical at the fourth-order point, occurring at the stability limit of tricriticality, given by  $p \approx 0.3288, D/J_{AB} \approx -2.1279$ , and  $k_B T/J_{AB} \approx 0.5659$ . In other words, the fourth-order point is located at the intersection of the line of tricritical points ( $T'$ ), the line of isolated critical points ( $C''$ ), and the line of critical end points ( $E$ ). Thus, for  $p < 0.3288$  an additional tricritical point ( $T'$ ) occurs at low temperatures on the line separating the paramagnetic phase from the ordered ones (this simple a fourth type phase diagram is not shown here). For  $p \approx 0.2443$ , the two tricritical points coalesce at  $D/J_{AB} \approx -1.8116$  and  $k_B T/J_{AB} \approx 0.6865$ . Thus for  $0 < p < 0.2443$  there is only a second-order transition separating the ferrimagnetic and paramagnetic phases, as can be seen in Fig. 10, where also a first-order  $[\frac{1}{2}, 1, -\frac{1}{2}]/[\frac{3}{2}, 1, -\frac{3}{2}]$  transition appears at low temperature. This low-temperature first-order phase transition starts at the value of  $D/J_{AB} \approx -1.2263$  satisfying  $D/J_{AB} = -6[p + 2R(1-p)]/[2 + 3(1-p)]$  (also see the inset of Fig. 10) and terminates at an isolated critical point ( $C$ ).

The tricritical behavior of the system discussed above is clearly shown in Fig. 11 where the solid line denotes projection of the stable tricritical line along the  $D/J_{AB}$  direction and the star indicates the position of the fourth-order point.

#### IV. CONCLUSIONS

In this work, for the first time we have determined the phase diagrams of the mixed ferromagnetic-ferrimagnetic

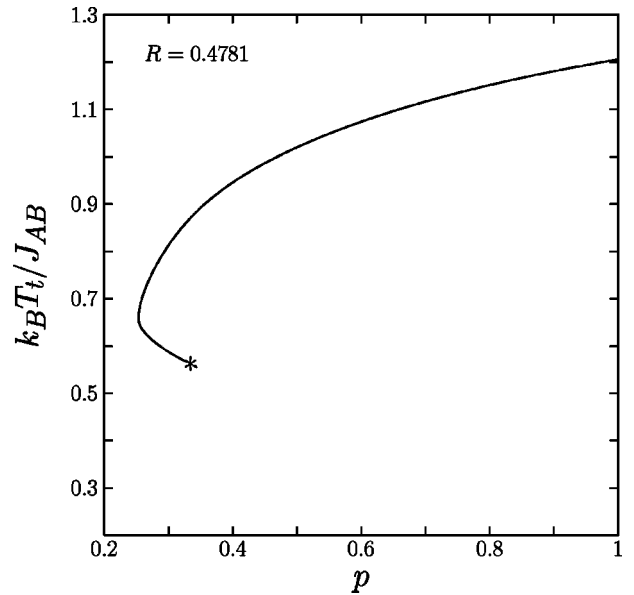


FIG. 11. Projection of the line tricritical points along the  $D/J_{AB}$  axis. The solid line represents the positions of stable tricritical points and the star corresponds to the projection of the fourth-order point.

ternary alloy composed of three different metal ions with spins  $\frac{3}{2}$ , 1, and  $\frac{5}{2}$  in the presence of an equal single-ion anisotropy strength for the three sublattices. The calculation was performed within the MFA based on the Bogoliubov inequality for the Gibbs free energy. Depending on the values of the parameters in the model Hamiltonian, the phase diagram in the  $D$ - $T$  plane exhibits a quite rich structure, with several multicritical points of various kinds. The highest-order multicritical entity is the fourth-order point. Thus, the model provides an unusually rich laboratory for studying a number of phase transitions, critical and multicritical phenomena within the framework of a one single approach.

To the best of our knowledge, the phase diagrams with fourth-order points have been obtained in the mean-field Ising model in the presence of a random field obeying a symmetric three-peak distribution,<sup>32</sup> the BEG model with a repulsive biquadratic coupling,<sup>33</sup> and the random-site binary ferromagnetic Ising model consisting of spin- $\frac{1}{2}$  and spin-1 with a single-ion anisotropy.<sup>34</sup> Therefore, the ternary alloy based on the Prussian blue analog with a single-ion anisotropy represents the another system which, at least according to the MFA, exhibits a fourth-order point.

Furthermore, one should notice that in the real  $AB_p C_{1-p}$  ternary alloy it may be reasonable to include at least two different anisotropy field strengths  $D_A$  and  $D_X$  on the spins  $S_A$  and  $S_X$  ( $X=B$  or  $C$ ), respectively. The inclusion of different anisotropies in the present method can be done straightforwardly, as has been accomplished in a corresponding study of the mixed spin-1 and spin- $\frac{3}{2}$  Ising system.<sup>27,28</sup> However, this could be a subject of a separate work.

Finally, we would like to point out that our results have the well-known deficiencies of the MFA. (It predicts, for instance, a zero value of the critical concentration for diluted magnets. Fortunately, this does not seem to be relevant for

the case of the ternary Prussian blue analog, where all sites are always occupied by the spins.) Moreover, the numerical calculations presented here were mostly restricted to the case  $R=R_c$ . Notwithstanding these limitations, we believe that the main qualitative conclusions, in particular those concerning the phase diagrams, are correct (also see the conclusion in Ref. 15) and some phenomena found in this work can be useful to understand the general properties of a ternary alloy. Of course, the accuracy of the obtained results could be further increased by using more reliable methods such as Monte Carlo simulations or the renormalization-group approach.

This is, however, a difficult task due to the complexity of the system in question. We wish this work would stimulate further experimental and theoretical investigations of multimetal Prussian blue analogs.

#### ACKNOWLEDGMENTS

This work was supported by the Scientific Grant Agency of Ministry of Education of Slovak Republic (Grant No. 1/9034/02) and Science and Technology Assistance Agency (Grant No. 20-009902).

\*Electronic address: abobak@kosice.upjs.sk

<sup>1</sup>*Magnetic Molecular Materials*, edited by D. Gatteschi, O. Kahn, J. S. Miller, and F. Palacio (Kluwer Academic, Dordrecht, 1991).

<sup>2</sup>O. Kahn, *Molecular Magnetism* (VCH, New York, 1993).

<sup>3</sup>J.S. Miller and A.J. Epstein, *Angew. Chem., Int. Ed. Engl.* **33**, 385 (1994).

<sup>4</sup>F. Palacio, G. Antorrena, M. Castro, R. Buriel, J. Rawson, J.N.B. Smith, N. Bricklebank, J. Novoa, and C. Ritter, *Phys. Rev. Lett.* **79**, 2336 (1997).

<sup>5</sup>M. Vardaguer, A. Bleuzen, V. Marvaud, J. Vaissermann, M. Seuleiman, C. Desplanches, A. Scullier, C. Train, R. Garde, G. Gelly, C. Lomenech, I. Rosenman, P. Veillet, C. Cartier, and F. Villain, *Coord. Chem. Rev.* **190-192**, 1023 (1999).

<sup>6</sup>H. Weihe and H.U. Güdel, *Comments Inorg. Chem.* **22**, 75 (2000).

<sup>7</sup>O. Kahn, Y. Pei, M. Verdaguer, J. Renard, and J. Sletten, *J. Am. Chem. Soc.* **110**, 782 (1988).

<sup>8</sup>H. Tamaki, Z.J. Zhong, N. Matsumoto, S. Kida, M. Koikawa, N. Achiva, Y. Hashimoto, and H. Okawa, *J. Am. Chem. Soc.* **114**, 6974 (1992).

<sup>9</sup>J.S. Miller, J.C. Calabrese, H. Rommelmann, S.R. Chittipeddi, J.H. Zhang, W.M. Reiff, and A.J. Epstein, *J. Am. Chem. Soc.* **109**, 769 (1987).

<sup>10</sup>J.M. Manriquez, G.T. Yee, R.S. McLean, A.J. Epstein, and J.S. Miller, *Science* **252**, 1415 (1991).

<sup>11</sup>M. Tamura, Y. Nakazawa, D. Shiomi, K. Nozawa, Y. Hosokoshi, M. Ishikawa, M. Takahashi, and M. Kinoshita, *Chem. Phys. Lett.* **186**, 401 (1991).

<sup>12</sup>P.M. Allemand, K.C. Khemani, A. Koch, F. Wudl, K. Holczer, S. Donovan, G. Grüner, and J.D. Thompson, *Science* **253**, 301 (1991).

<sup>13</sup>S. Ohkoshi, S. Yorozu, O. Sato, T. Iyoda, A. Fujishima, and K. Hashimoto, *Appl. Phys. Lett.* **70**, 1040 (1997).

<sup>14</sup>S. Ohkoshi, T. Iyoda, A. Fujishima, and K. Hashimoto, *Phys. Rev. B* **56**, 11 642 (1997).

<sup>15</sup>S. Ohkoshi and K. Hashimoto, *Phys. Rev. B* **60**, 12 820 (1999).

<sup>16</sup>S. Ohkoshi, Y. Abe, A. Fujishima, and K. Hashimoto, *Phys. Rev. Lett.* **82**, 1285 (1999).

<sup>17</sup>V.V. Kostyuchenko and A.K. Zvezdin, *J. Magn. Magn. Mater.* **258-259**, 548 (2003).

<sup>18</sup>O. Sato, T. Iyoda, A. Fujishima, and K. Hashimoto, *Science* **272**, 704 (1996).

<sup>19</sup>D.A. Pejakovic, J.L. Manson, J.S. Miller, and A.J. Epstein, *Current Appl. Phys.* **1**, 15 (2001).

<sup>20</sup>S. Ohkoshi and K. Hashimoto, *J. Am. Chem. Soc.* **121**, 10 591 (1999).

<sup>21</sup>S. Ohkoshi, T. Hozumi, and K. Hashimoto, *Phys. Rev. B* **64**, 132404 (2001).

<sup>22</sup>A. Bobák, O.F. Abubrig, and D. Horváth, *Physica A* **312**, 187 (2002).

<sup>23</sup>J.W. Tucker, T. Balcerzak, M. Gzik, and A. Sukiennicki, *J. Magn. Magn. Mater.* **187**, 381 (1998).

<sup>24</sup>A. Bobák, T. Balcerzak, and F.O. Abubrig, *Physica A* **326**, 151 (2003).

<sup>25</sup>Y. Nakamura, *Phys. Rev. B* **62**, 11 742 (2000).

<sup>26</sup>S.G. Carling and P. Day, *Polyhedron* **20**, 1525 (2001).

<sup>27</sup>A. Bobák, *Physica A* **258**, 140 (1998).

<sup>28</sup>O.F. Abubrig, D. Horváth, A. Bobák, and M. Jaščur, *Physica A* **296**, 437 (2001).

<sup>29</sup>H. Falk, *Am. J. Phys.* **38**, 858 (1970).

<sup>30</sup>J.A. Plascak, J.G. Moreira, and F.C. Sá Barreto, *Phys. Lett. A* **173**, 360 (1993).

<sup>31</sup>J.W. Tucker, *J. Magn. Magn. Mater.* **214**, 121 (2000).

<sup>32</sup>M. Kaufman, P.E. Klunzinger, and A. Khurana, *Phys. Rev. B* **34**, 4766 (1986).

<sup>33</sup>W. Hoston and A.N. Berker, *Phys. Rev. Lett.* **67**, 1027 (1991).

<sup>34</sup>J.A. Plascak, *Physica A* **198**, 655 (1993).